Smooth Reverse Loop and Catmull-Clark Subdivision

Javad Sadeghi*, Faramarz F. Samavati

Department of Computer Science, University of Calgary, Alberta, Canada

Abstract

In this paper we present a new multiresolution technique for general topology surfaces based on reversing subdivision with energy minimization. We first introduce a general reverse subdivision approach that starts from a trial set of biorthogonal multiresolution filters and refines the resulting coarse points using local masks. The refinement step tries to find a good approximation of the fine points while minimizing the local energy of the coarse points in a least-squares sense. This approach is then used to find smooth reverse of the Loop and Catmull-Clark subdivisions. We discuss the advantages of using this technique in various surface editing and synthesis applications.

Keywords: multiresolution, reverse subdivision, energy minimization, Loop subdivision, Catmull-Clark subdivision

1. Introduction

Subdivision techniques are now widely used in modeling applications. An artist or modeler can create an object in a coarse level and subdivide it efficiently to a smoother representation. On the other hand, multiresolution (MR) techniques can be used to find a coarse approximation of a fine object in a process called *decomposition*. This process can be constructed by reversing the subdivision rules. However, when the high-resolution data is not directly resulted from subdivision, some additional information should be stored at every level of decomposition. This extra information or error is captured as detail vectors by a linear combination of functions known as

---

*Corresponding author

Email addresses: jsadeghi@ucalgary.ca (Javad Sadeghi), samavati@ucalgary.ca (Faramarz F. Samavati)
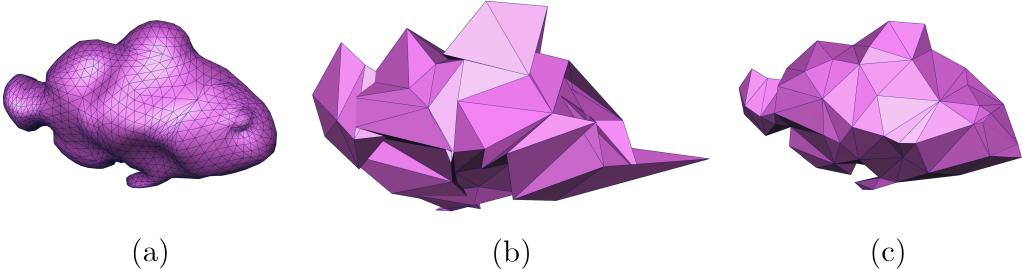
(a)　　　　　　　　(b)　　　　　　　　(c)

Figure 1: (a) A model with $2,752$ faces. (b) Reverse Loop subdivision. (c) Smooth reverse Loop subdivision.

wavelets. Details are then used to generate the original fine data in a process called *reconstruction*. Since detail vectors contain the high-energy portion of the models they are usually considered as representatives of the key characteristics of the objects.

Details resulted from MR, play an important role in example-based applications. In these applications details of a high-resolution model are extracted and then re-applied to a different low-resolution base model. In the conventional techniques for MR, details are not necessarily a good representative of the characteristics information of the fine points. They may contain some positional information to compensate the extra deviations of the coarse points during decomposition. Consequently, the resulting by-example techniques from these kinds of MR may not provide high-quality synthesized models. Therefore, if we can extract details that better approximate characteristics of the high-resolution objects, we would be able to synthesize objects with more precise characteristics. As pointed out in [1] and [2], in order to have details with the best characteristics, it is necessary to have a low energy (smooth) coarse approximation of the high-resolution model.

Since subdivision is a smoothing operation its reverse may create a high-energy coarse approximation. Therefore, after some levels of decomposition it is usually hard to find a correspondence between the overall structure of the coarse points and the original fine points. Fig. 1 shows a fine mesh with $2,752$ faces and its second level of decomposition using two different reverse subdivision techniques. As shown, the coarse mesh in Fig. 1(b) is not a good choice for MR editing applications. For example, it is hard to scale the lower fin of the fish model because the related vertices are not visible enough and also their correspondence with the original fine mesh is hard to

determine. In contrast, the smooth coarse mesh in Fig. 1(c) preserves the overall structure of the original fine mesh which makes it a better choice for MR editing applications.

Recently, Sadeghi and Samavati [3] introduced a reverse subdivision technique mostly for curves and simple multivariate meshes that considers the smoothness of the coarse points as a factor in the decomposition process. In their framework two goals of preserving a good approximation of the fine points and reducing the energy of the coarse points are balanced in a global least squares sense. While their approach improves current curve synthesis and tensor-product surface synthesis applications, it is not clear how it can be extended to general topology surfaces. The main reason is that their decomposition operation acts globally on the entire high-resolution points to create low-resolution points and details. Therefore, for a small perturbation of the fine points (e.g. relocation of a fine point) all of the low-resolution and consequently all of the details are involved. However, subdivision surfaces are constructed through local masks and it is desired that the corresponding reverse subdivision (RS) be created through local operations. This limitation of Sadeghi and Samavati's work motivated us to focus on constructing local MR operations in order to extend their approach to subdivision schemes of general topology surfaces.

This paper contributes a novel multiresolution technique for arbitrary topology surfaces, Loop [4] and Catmull-Clark [5], based on reversing subdivision with energy minimization of the coarse mesh. In our method we first apply a trial set of reverse subdivision filters to a fine mesh with subdivision connectivity and then refine the resulting coarse mesh using weighted local least-squares to minimize its local subdivision error and local energy. The refined coarse mesh in our approach better preserves the overall structure of the fine mesh. This improves the MR editing of the fine mesh. Also our approach creates more meaningful residuals for synthesizing applications. We take advantage of a compact representation for MR setting and have linear processing time for all of the MR operations. The effectiveness of our approach is demonstrated through example mesh editing and synthesis applications.

The paper is organized as follows: In section 2 the related work to this research is reviewed. Details of our construction method is covered in section 3. Section 4 demonstrates flexibility of our approach with different multiresolution schemes for general topology surfaces. In section 5 some example results of our method are discussed. Finally, section 6 concludes the paper

and proposes the future directions.

2. Related work

In a multiresolution representation a set of fine points C^n is decomposed to a set of coarse points C^{n-1} and some wavelet coefficients D^{n-1} called details. The decomposition is done using *analysis filter matrices* A^n and B^n as

$$
\begin{aligned}
C^{n-1} &= A^n C^n \\
D^{n-1} &= B^n C^n.
\end{aligned}
\tag{1}
$$

Detail vectors allow the original fine points to be restored using *synthesis filter matrices* P^n and Q^n in the reconstruction process as

$$
C^n = P^n C^{n-1} + Q^n D^{n-1}.
\tag{2}
$$

In a biorthogonal multiresolution system the MR filters A^n, B^n, P^n and Q^n satisfy the biorthogonality condition

$$
\left[\frac{A^n}{B^n} \right] [P^n | Q^n] = \left[\begin{array}{cc} I & 0 \\ 0 & I \end{array} \right] = I
\tag{3}
$$

that implies the reconstruction is inverse of the decomposition [6]. C^n can be decomposed repeatedly several times to create a hierarchy of coarse points C^l, C^{l+1}, ..., C^{n-1} and details D^l, D^{l+1}, ..., D^{n-1} where $l < n$.

Samavati and Bartels [7] pioneered an approach for multiresolution by reversing the subdivision rules with least-squares data fitting. Their method ensures that subdivision of the low-resolution model is a good approximation of the high-resolution model. They construct the global least squares formulation

$$
min \left\| C^n - PC^{n-1} \right\|_2^2
\tag{4}
$$

to obtain the C^{n-1} and a compact representation of residuals with corresponding A^n, B^n and Q^n in linear time. Later, Bartels and Samavati [8] improved this approach by deriving local reverse subdivision filters using local linear conditions (LLC). Then Samavati et al. [9] used this local approach to construct multiresolution filters for Doo-Sabin [10] subdivision surface. The derived filters are sparse and result in a coarse surface which is locally closest to the original fine surface in a local least squares sense.

4

Multiresolution systems have been successfully used in a number of applications on curves and surfaces. Finkelstein and Salesin [11] describe a wavelet-based multiresolution representation to support variety of display and editing operations on curves. Kobbelt and Schröder [12] present a multiresolution setting based on interpolating subdivision schemes for making variationally optimal curves and associated wavelets. Lounsbery et al. [13] use wavelet representations based on subdivision surfaces for variety of multiresolution applications on compact surfaces with arbitrary topology. Kobbelt et al. [14] develop a multiresolution technique for interactive detail-preserving mesh modification based on incremental mesh decimation and discrete fairing. They deform a smoothed region of an arbitrary triangular mesh which does not require having subdivision connectivity and add back the details. However, the non-uniform parameterization of the meshes in their hierarchical setting generates large detail vectors. They have to change the connectivity of the smoothed mesh in order to reduce the number of the pathological configurations. Even after this refinement some artifacts are observed on their reconstructed high-frequency surfaces because they do not optimize the corresponding detail vectors. Zorin et al. [15] demonstrate a set of algorithms for interactive MR editing of the meshes with subdivision connectivity. In their work dynamic manipulation of the vertices at a smooth coarse level makes topological edits to the mesh. As the authors stated, their smoothing filters are not the dual of subdivision filters (Loop). Therefore, their smoothing lacks a local shape control and magnifies the low frequency surface features. This has a negative impact on the quality of their detail vectors. Samavati et al. [16] have constructed a more efficient MR system by reversing Loop subdivision. They also reverse the texture-mapping process of the multiresolution surfaces. Lanquentin and Neveu [17] have constructed a reversal method for Catmull-Clark subdivision by solving a linear system of equations. Both of the [16] and [17] only derive the reverse operation A and the other operations of MR are not derived.

Bertram [18] constructs biorthogonal wavelets for Loop subdivision based on the lifting scheme [19]. He rewrites the subdivision rules with some additional free parameters in a way that regular subdivision is unchanged but an inversion of the rules produces a MR system. Bertram [20] also provides biorthogonal wavelet construction for MR modeling of large-scale isosurfaces using Catmull-Clark subdivision. The computation of this wavelet transform is based on the local lifting-style filtering operations. Li et al. [21] construct fairly stable biorthogonal wavelets for Loop subdivision in a similar way to

Bertram but with simpler representation especially around the extraordinary vertices. Although these techniques improve the speed of the wavelet analysis, their performance depends heavily on a variety of free parameters. Olsen et al. [22] utilize the distinction between even and odd vertices of subdivision schemes to find a set of trial filters, similar to lazy wavelets. These trial filters are then refined locally by an optimization step to reduce the decomposition error. This approach is demonstrated for cubic B-spline curves and Loop subdivision surfaces. Later, Olsen and Samavati [23] could find discrete MR construction for variety of subdivision schemes including Dyn-Levin-Gregory curves and Catmull-Clark surfaces. The last two approaches ([22] and [23]) provide a compact and efficient representation for multiresolution setting without any direct use of wavelets. However, the detail vectors in these techniques are not a good representative for characteristics information because the energy of the coarse data is not minimized.

Manipulating a surface while preserving its geometric details is a crucial part of many surface editing applications. Forsey and Bartels [24] introduce a uniform framework for editing shapes at various levels of details based on hierarchical B-spline refinement (H-splines). The main limitation of H-splines is that they can only represent parametric and tensor-product surfaces. Eck et al. [25] provide a mesh simplification algorithm based on harmonic maps for various MR applications on arbitrary meshes including: compression, powerful editing and level-of-detail control. Their algorithm causes some distortion because they compute global smooth parameterizations for a coarse base domain rather than using a local neighborhood. Lee et al. [26] attempt to address this issue by hierarchical parameterization of the original mesh over the base domain containing a small number of triangles. They use fully automatic and user constrained remeshing operations to achieve a mesh with subdivision connectivity suitable for MR editing. Biermann et al. [27] present a MR-based feature transfer algorithm for Catmull-Clark surfaces. Feature transfer is a way of editing a model using the characteristics of other models. As stated in [1] the best feature transfer results are achieved when all of the high-energy data is stored in the details. In order to store all of the characteristics information in details we need a multiresolution system that creates smooth coarse points.

Taubin [28] derives Laplace smoothing operator based on generalized Fourier analysis for arbitrary topology surfaces. His algorithm reduces the problem of mesh fairing to low-pass filtering and produces smoothing without shrinkage. Sorkine et al. [29] provide an interactive detail preserving

surface editing technique based on rotation and scale invariant Laplacian coordinates. This technique is used for feature transfer as well as mixing, and transplanting partial surface meshes. None of [28] and [29] support hierarchical representation for details. Kobbelt et al. [30] enable true free form MR editing with suitable detail encoding for arbitrary meshes with no restrictions on the connectivity. They first find a smooth base surface using constrained discrete fairing. Then define the high-resolution mesh based on the normal displacements of the low-frequency vertices. However, in the multi-level smoothing step of their method they iteratively solve a global system using Gauss-Seidel scheme that is costly and time consuming for a minimum-error approximation. In contrast, a fast multi-level smoothing results in smooth coarse approximation which does not preserve the overall structure of the fine mesh and consequently is not suitable for MR editing. In general, the MR techniques that remove the subdivision connectivity constraint need extra optimization steps which are better justified in the category of progressive meshes. In addition, the subdivision connectivity can be achieved by remeshing or by the advent of the new sketch-based techniques that directly build freeform surfaces with subdivision connectivity [31, 32]. Using these techniques we can avoid the extra optimization steps in the MR construction.

Recently, Sadeghi and Samavati [3] have considered smoothness of the coarse points in the reverse subdivision technique. They start their construction from a trial set of multiresolution filters and use a global least squares formulation to minimize the energy of the coarse points while reducing the subdivision error. By enhancing the results in real-time, full set of biorthogonal MR operations are constructed in the form of banded matrices. Although the result of using this approach in synthesizing applications seems promising, they do not discuss the possibility of extending their approach to general topology surfaces. As discussed in section 1, they use a global optimization technique for MR that cannot be naturally extended to multiresolution representation for general topology surfaces. The main reason for this deficiency is the lack of local operations to support smooth reverse subdivision. Therefore, by finding a local RS approach that minimizes the energy of the coarse points we can extend their work to MR techniques for general topology surfaces (Loop and Catmull-Clark).

3. Construction method

In this section we describe our local RS approach to find coarse models with minimum subdivision error and minimum energy. Our construction is demonstrated in detail for cubic B-spline curves. We will use this approach later in section 4 for MR construction of common surface subdivision schemes.

3.1. General approach

Here we describe our general approach for including the smoothness of the coarse points in the MR construction. As discussed in section 1, the resulting smooth coarse models preserve the overall structure of the fine models. Since reverse subdivision schemes for general topology surfaces are built through local operations we need to find a local MR approach that satisfies our optimization goals.

In our construction we first find local MR masks for the given subdivision scheme. This can be done in various ways; we use an approach similar to LLC [8] by constructing MR for a local neighborhood of the data points. We can start from neighborhoods with different sizes to find the local subdivision mask P. From P we can derive trial multiresolution masks $\widetilde{A}$, $\widetilde{B}$ and $\widetilde{Q}$. Then we refine the coarse vertices resulted from trial mask $\widetilde{A}$ locally in a least squares sense to satisfy our desired optimization goals. From this refinement, the multiresolution masks are modified respectively. Due to the uniformity of subdivision, the least squares solution form a local mask that can be used *repetitively* on different locations to cover the entire data points. Therefore, we do not need to solve this local least squares again for all of the coarse points. As discussed in detail by Bartels et al. [33], the global least squares solution is well estimated by this local least squares solution and the estimation rapidly improves with the size of the local least squares problems.

To simplify our notation we focus only on one decomposition and reconstruction step. We start from a local set of fine points F and find trial coarse points $\widetilde{C}$ and trial detail vectors $\widetilde{D}$ locally using $\widetilde{A}$ and $\widetilde{B}$ respectively. For a coarse point such as $\widetilde{c}_i$, we localize the construction of MR in a local neighborhood $N(i)$ (indices of neighboring vertices of $\widetilde{c}_i$). We would like to change the trial coarse points $\widetilde{C}$ to their final position C by using a perturbation vector $\Delta = [\delta_j]$ as

$$
\begin{cases}
c_j = \widetilde{c}_j + \delta_j & j \in N(i) \\
c_j = \widetilde{c}_j & j \notin N(i).
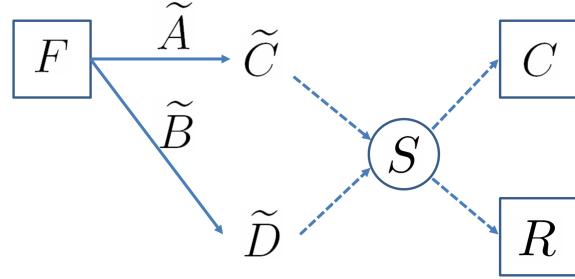\end{cases}
\tag{5}
$$

Figure 2: Decomposition process of local smooth reverse subdivision.

The goal is to minimize

$$E_{total}(\Delta) = \omega E_{subdiv}(\Delta) + (1 - \omega)E_{energy}(\Delta) \tag{6}$$

where $E_{subdiv}(\Delta)$ denotes the Euclidean distance between PC and F known as *residuals*

$$R = F - PC \tag{7}$$

and $E_{energy}(\Delta)$ denotes the energy of C in the local neighborhood. The weight parameter $0 \leq \omega \leq 1$ controls the importance of the subdivision fitness versus energy minimization.

Eq. (6) is a local weighted least squares problem and can be solved one time for the local neighborhood. To obtain all of the coarse points, the local window should be formed for all valid i values (and for all of the resolutions). Depending on the width of the neighborhood, local windows for nearby points can collide and consequently it is possible to obtain multiple perturbation vectors per point. Approaches similar to [9] can be employed to use these multiple perturbations to lower E_{subdiv} in construction of MR. However, such techniques make our approach for finding a *reverse subdivision mask* that also includes E_{energy} very complicated. Therefore, for preventing this multiplicity we only perturb the central vertex $\widetilde{c}_i$ by vector δ_i.

Fig. 2 demonstrates our decomposition process with the optimization step denoted by S. R contains the residual vectors necessary to reconstruct the original fine points.

In our reconstruction process we can generate the original fine points from the trial coarse points and trial details

$$F = P\widetilde{C} + \widetilde{Q}\widetilde{D}. \tag{8}$$

If it is important to keep the residuals (e.g. in synthesizing applications), F is found from Eq. (7).

The advantage of this local approach is that we have a compact representation which is extensible to the subdivision schemes for general topology surfaces.

3.2. Cubic B-spline

To demonstrate the general approach in a simple example scheme, we explain details of our construction for cubic B-spline curves. We will use the local cubic B-spline smooth reverse subdivision later in section 4 for boundary treatment of smooth reverse Loop and Catmull-Clark subdivisions.

Cubic B-spline is an important primal (edge-split) scheme that displaces even vertices and creates odd vertices at the midpoint of the edges. We start our construction from trial cubic B-spline MR filters [34]

$$
\begin{aligned}
\mathbf{a} &= \begin{bmatrix} -\frac{1}{2} & 2 & -\frac{1}{2} \end{bmatrix} \\
\mathbf{b} &= \begin{bmatrix} \frac{1}{4} & -1 & \frac{3}{2} & -1 & \frac{1}{4} \end{bmatrix} \\
\mathbf{p} &= \begin{bmatrix} \frac{1}{8} & \frac{1}{2} & \frac{3}{4} & \frac{1}{2} & \frac{1}{8} \end{bmatrix} \\
\mathbf{q} &= \begin{bmatrix} \frac{1}{4} & 1 & \frac{1}{4} \end{bmatrix}
\end{aligned}
\tag{9}
$$

in a local neighborhood of width seven fine points. For more accurate approximation we can start with larger neighborhoods. In order to have symmetric indexing in this neighborhood we denote fine points by $F = \{f_{-3}, f_{-2}, f_{-1}, f_0, f_1, f_2, f_3\}$ and the trial coarse points by $\widetilde{C} = \{\widetilde{c}_{-1}, \widetilde{c}_0, \widetilde{c}_1\}$. Fig. 3 shows the local neighborhood of seven fine points and corresponding trial coarse points. This configuration is formed to determine local filters corresponding to the center point $\widetilde{c}_0$. Therefore, we have two trial detail vectors in this neighborhood that when multiplied by $\widetilde{Q}$ will provide three trial residuals denoted by $\widetilde{R} = \{\widetilde{r}_{-1}, \widetilde{r}_0, \widetilde{r}_1\}$ as shown in Fig. 3.

Our goal is to minimize the discrete curve energy of the final coarse curve in this neighborhood. To approximate the curve energy around c_0 we use discrete Laplacian definition [28]

$$
\Delta c_0 = c_{-1} - 2c_0 + c_1.
\tag{10}
$$

Hence, as used in [3] we can formulate the local energy minimization goal as

$$
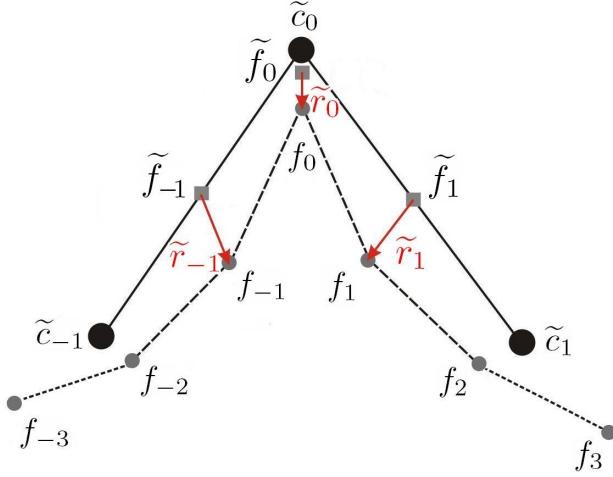E_{energy}(\delta_0) = \|c_{-1} - 2c_0 + c_1\|_2^2.
\tag{11}
$$

Figure 3: Notation for decomposition of the fine points f_i to the coarse points $\widetilde{c}_i$ in a neighborhood of seven fine points using trial cubic B-spline filters. Red arrows denote trial residuals. Subdivided coarse points are denoted by $\widetilde{f}_i$.

As mentioned in section 3.1 in order to prevent multiple perturbations we set $c_{-1} = \widetilde{c}_{-1}$ and $c_1 = \widetilde{c}_1$ which helps to re-write our energy error in terms of δ_0 as

$$E_{energy}(\delta_0) = \|\widetilde{c}_{-1} - 2(\widetilde{c}_0 + \delta_0) + \widetilde{c}_1\|_2^2. \tag{12}$$

To approximate the subdivision error in the local neighborhood we use a notation based on the final residuals (R)

$$E_{subdiv}(\delta_0) = \|r_{-1}\|_2^2 + \|r_0\|_2^2 + \|r_1\|_2^2. \tag{13}$$

The displacement of $\widetilde{c}_0$ by δ_0 changes the positions under act of the subdivision. Therefore, we can re-write Eq. (13) in terms of the trial residuals and the perturbation vector δ_0 as

$$
\begin{aligned}
E_{subdiv}(\delta_0) &= \left\| f_{-1} - \left(\widetilde{f}_{-1} + \frac{1}{2}\delta_0 \right) \right\|_2^2 + \left\| f_0 - \left(\widetilde{f}_0 + \frac{3}{4}\delta_0 \right) \right\|_2^2 \\
&\quad + \left\| f_1 - \left(\widetilde{f}_1 + \frac{1}{2}\delta_0 \right) \right\|_2^2 = \left\| \widetilde{r}_{-1} - \frac{1}{2}\delta_0 \right\|_2^2 \\
&\quad + \left\| \widetilde{r}_0 - \frac{3}{4}\delta_0 \right\|_2^2 + \left\| \widetilde{r}_1 - \frac{1}{2}\delta_0 \right\|_2^2. \tag{14}
\end{aligned}
$$

11

Now both E_{subdiv} and E_{energy} are in terms of δ_0 and this refinement vector is found from solving the weighted least squares in Eq. (6).

In order to have more economic representation for the residuals, we can use the idea of constrained wavelets [22]. Using the inherent structure of subdivision schemes, the fine points are broken up to two disjoint sets even/odd. Then after decomposition, vertices labeled as "even" are replaced with a point in the coarse resolution and vertices labeled as "odd" with a corresponding entity from the details. Because of the linear and local nature of subdivision schemes, even details can be computed by a linear combination of the odd details. In the case of cubic B-spline we have

$$\widetilde{d}_0 = \frac{1}{4}(\widetilde{d}_{-1} + \widetilde{d}_1). \tag{15}$$

The advantage of this approach is that coarse points and details will not take more space than the fine points. Using Eq. (7) and (15) we can simplify Eq. (14) as

$$E_{subdiv}(\delta_0) = \frac{17}{16}\|\delta_0\|_2^2 - \frac{11}{8}(\widetilde{d}_{-1} + \widetilde{d}_1)\delta_0 + \left\|\widetilde{d}_{-1}\right\|_2^2 + \left\|\widetilde{d}_0\right\|_2^2 + \left\|\widetilde{d}_1\right\|_2^2. \tag{16}$$

Now we can use E_{subdiv} in Eq. (6) and solve the local least squares formulation to find δ_0 as

$$\delta_0 = \frac{11\omega}{64 - 47\omega}(\widetilde{d}_{-1} + \widetilde{d}_1) + \frac{32 - 32\omega}{64 - 47\omega}(\widetilde{c}_{-1} - 2\widetilde{c}_0 + \widetilde{c}_1). \tag{17}$$

The final coarse point c_0 is obtained from $c_0 = \widetilde{c}_0 + \delta_0$.

By changing the center of the local neighborhood and repeating the above steps we can find any c_i in C. Notice that it is not necessary to solve the local least squares problem for all the coarse points, but Eq. (17) can be used as a mask-like operation. Obviously, perturbing the coarse points alters the residuals. After finding C, the final residuals can be found from Eq. (7). Using R and the final coarse points we can reconstruct the fine points.

Fig. 4 shows a face profile with 96 points and three levels of its local cubic B-spline smooth reverse subdivision. As shown, it gradually loses its energy during reduction of the resolution by reverse subdivision.

Fig. 5 compares extracting and re-using details of the face profile in Fig. 4(a) using local cubic B-spline RS filters introduced by Bartels and Samavati

(a) 96 points   (b) 48 points   (c) 24 points   (d) 12 points
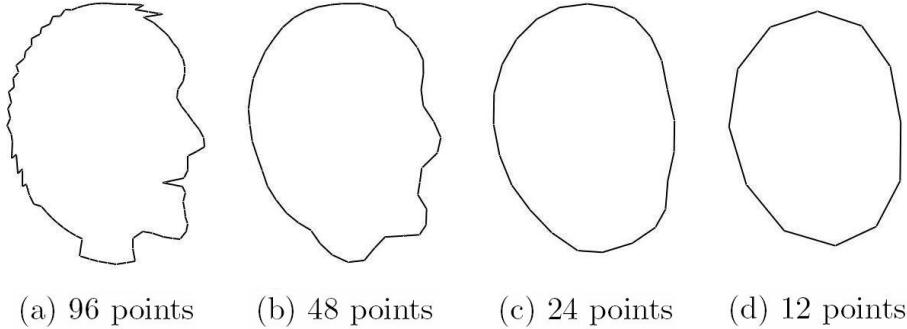
Figure 4: A closed curve with 96 points and its three levels of local cubic B-spline smooth reverse subdivision.

[8] and local cubic B-spline smooth reverse subdivision. Fig. 5(a) visualizes the first level of the residual vectors (the green lines) as differences between the fine points in Fig. 4(a) and subdivision of the coarse points (the blue curve) using Bartels and Samavati's filters. Fig. 5(b) visualizes the residual vectors obtained in a similar way using our approach. We then replace the coarse points with an ellipse containing 48 points (see Fig. 5(c)). Fig. 5(d) shows the synthesized curve using Bartels and Samavati's filters while Fig. 5(e) shows similar synthesis result using local cubic B-spline smooth reverse subdivision. Due to the smoothness of the coarse points in our approach, detail vectors capture the characteristics of the curve more precisely. This can be verified by comparing the right side of the curves in Fig. 5(d) and Fig. 5(e).

When we change the base path of the original curve, it is necessary to transfer details with the same orientation to the new path. In order to properly re-orient original details at destination points we use the method introduced by Forsey and Bartels [24]. We first create a local parallel transport frame [35] at each point on the curve. Then convert the world coordinates of the detail vectors to that local frame in order to have a local coordinate. During reconstruction, the orientation of these local details will be aligned with the corresponding local frame on the new curve.

All of the previous discussions were based on the regular cubic B-spline filters. For smooth reverse Loop and Catmull-Clark subdivisions (section 4) we sometimes need to treat the points lying on a crease or boundary of the surface as an open curve. Here we discuss how our approach can be extended
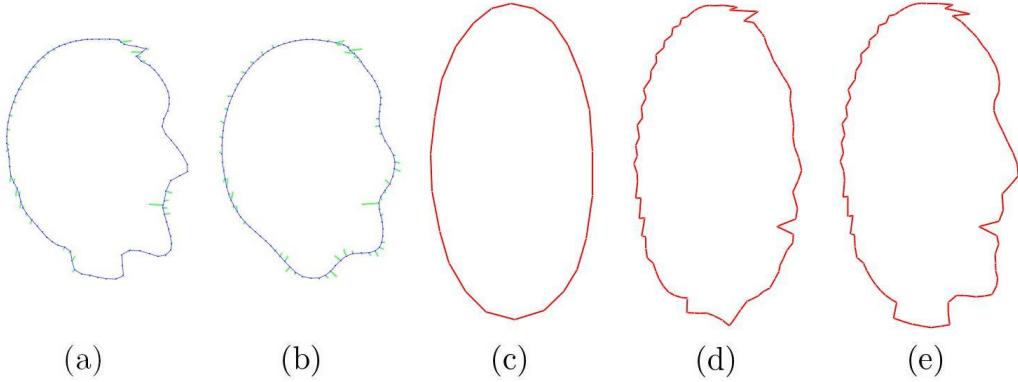
13

Figure 5: (a) Residual vectors using Bartels and Samavati's cubic B-spline RS filters. (b) Residual vectors using local cubic B-spline smooth reverse subdivision. (c) New base path with 48 points. (d) Synthesized model using Bartels and Samavati's filters. (e) Synthesized model using our approach.

to the curves with boundaries. We start our boundary construction from the short cubic B-spline boundary scheme [34] and use our general approach for refinement. We need to use a different local indexing for the boundaries as $C = \{c_0, c_1, c_2\}$ and $F = \{f_0, f_1, f_2, f_3, f_4, f_5, f_6\}$. Based on this setting, the extra-ordinary vertices at the beginning of the curve are expressed as

$$
\begin{aligned}
\widetilde{f_0} &= \widetilde{c_0} \\
\widetilde{f_1} &= \frac{1}{2}\widetilde{c_0} + \frac{1}{2}\widetilde{c_1} \\
\widetilde{f_2} &= \frac{3}{4}\widetilde{c_1} + \frac{1}{4}\widetilde{c_2} \\
\widetilde{f_3} &= \frac{3}{16}\widetilde{c_1} + \frac{11}{16}\widetilde{c_2} + \frac{1}{8}\widetilde{c_3}.
\end{aligned}
\tag{18}
$$

Since $\widetilde{Q}$ in [34] is just defined for regular case, using Eq. (7) and (8) we obtain $\widetilde{r}_0 = \widetilde{r}_1 = 0$. This means that $f_0 = \widetilde{f_0}$ and $f_1 = \widetilde{f_1}$. Since we usually clamp the start and end points of an open curve in MR, we ignore E_{energy} and only minimize E_{subdiv} to interpolate the position of $c_0 = \widetilde{c_0}$. This allows $\widetilde{c_1}$ to be determined without error as $c_1 = \widetilde{c_1} = 2f_1 - f_0$. Since we do not perturb the first two trial coarse points we have $\delta_0 = \delta_1 = 0$. In order to find the refinement vector associated with $\widetilde{c_2}$ we approximate subdivision error in the local neighborhood of the first seven fine points using an equation similar

14

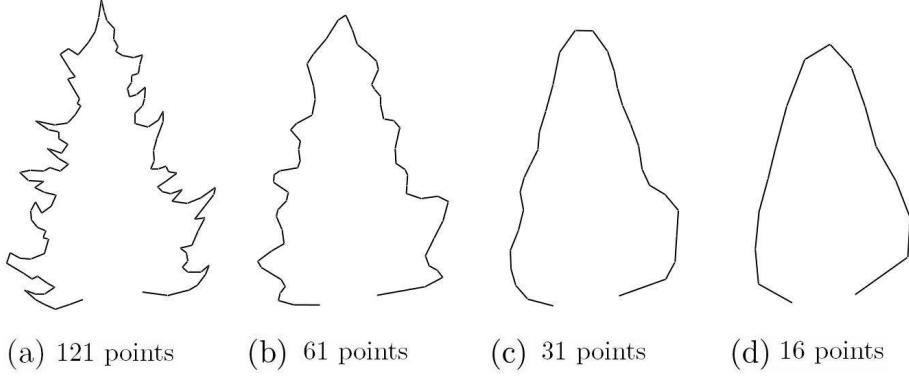(a) 121 points   (b) 61 points   (c) 31 points   (d) 16 points

Figure 6: An open curve with 121 points and its three levels of local cubic B-spline smooth reverse subdivision.

to Eq. (14). The energy term is calculated similar to Eq. (11). By solving the resulted weighted least squares we can find δ_2 and c_2.

Using constrained wavelets' notation presented in Eq. (15) we can simplify representation of the subdivision error as

$$
\begin{aligned}
E_{subdiv}(\delta_2) &= \frac{201}{256}\|\delta_2\|_2^2 - (\frac{27}{32}\widetilde{d}_2 + \frac{43}{32}\widetilde{d}_4)\delta_2 + \\
&\quad \left\|\widetilde{d}_2\right\|_2^2 + \left\|\widetilde{d}_3\right\|_2^2 + \left\|\widetilde{d}_4\right\|_2^2
\end{aligned}
\tag{19}
$$

and the final δ_2 as

$$
\delta_2 = \frac{128\omega}{1024 - 823\omega}(\frac{27}{32}\widetilde{d}_2 + \frac{43}{32}\widetilde{d}_4) + \frac{512 - 512\omega}{1024 - 823\omega}(\widetilde{c}_1 - 2\widetilde{c}_2 + \widetilde{c}_3).
\tag{20}
$$

The refinement vector for any other regular $\widetilde{c}_i$ is calculated from Eq. (17) by centering the neighborhood on $\widetilde{c}_i$. Due to the symmetrical situation, we can construct extra-ordinary points at the end of the curve in a similar way to our construction at the beginning of the curve. After finding C we can find the final residual vectors from Eq. (7) using boundary masks expressed in Eq. (18).

Fig. 6 shows an example of applying our local cubic B-spline smooth reverse subdivision boundary filters tree times to an open tree profile. It shows that smooth low-resolution curves follow overall structure of the original curve. The general approach we presented in section 3.1 can be used in

15

a similar way for other curve schemes such as Chaikin [36] and Dyn-Levin-Gregory [37]. Bartels and Samavati have introduced local trial Chaikin reverse subdivision filters at [8]. Also the MR setting of Olsen and Samavati [23] can be used as trial filters for local Dyn-Levin-Gregory smooth reverse subdivision.

4. Subdivision surface schemes

In this section we use the general approach introduced in section 3.1 to derive our MR representations for general topology surfaces. The local nature of our approach allows us to extend it to surfaces with arbitrary topology. Here we present details of our construction for smooth reverse Loop and Catmull-Clark subdivision schemes.

4.1. Loop subdivision

Loop subdivision [4] is a subdivision scheme for triangular meshes with C^2 continuity at the regular vertices. It splits each triangular face into four new triangles and smoothly repositions the resulting vertices using positional masks.

As discussed in section 3.1, in order to construct local smooth reverse subdivision we need to start from a set of trial masks P, $\widetilde{Q}$, $\widetilde{A}$ and $\widetilde{B}$ in a local neighborhood of the given subdivision scheme. For Loop subdivision the local neighborhood is imposed by the local trial masks of Loop subdivision. In our work we start from Olsen et al.'s [22] compact trial masks for Loop subdivision. Then refine them to find coarse points that are good approximations of the fine points and have minimum surface energy in their local neighborhood. The local neighborhood on the surface is a 1-ring of the coarse vertices denoted by $\widetilde{C} = \{\widetilde{c}_0, \widetilde{c}_1, \ldots, \widetilde{c}_{n-1}, \widetilde{c}_n\}$. In this 1-ring neighborhood as shown in Fig. 7, by centering the Loop subdivision masks around the coarse vertex $\widetilde{c}_0$ with valence n the *vertex-vertex* (even) mask is defined as

$$\widetilde{f}_0 = (1 - n\beta)\widetilde{c}_0 + \beta \sum_{i=1}^{n} \widetilde{c}_i \tag{21}$$

where $\beta = \frac{1}{n}\left(\frac{5}{8} - \left(\frac{3}{8} + \frac{1}{4}\cos\left(\frac{2\pi}{n}\right)\right)^2\right)$ and *edge-vertex* (odd) mask for $i = 1, 2, \ldots, n$ is defined as

$$\widetilde{f}_i = \frac{3}{8}(\widetilde{c}_0 + \widetilde{c}_i) + \frac{1}{8}(\widetilde{c}_{i-1} + \widetilde{c}_{i+1}). \tag{22}$$
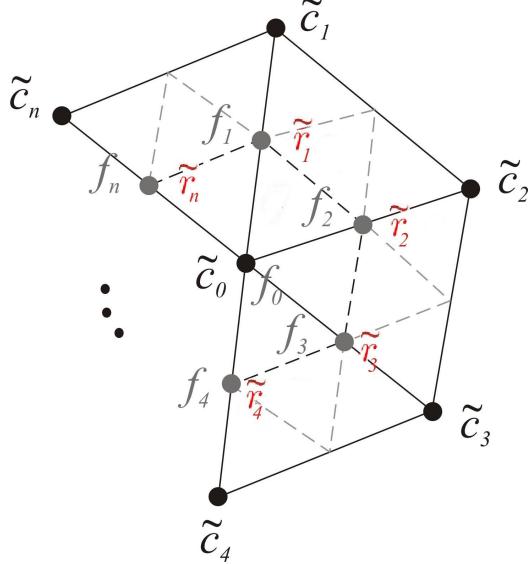
16

Figure 7: Notation for the reverse Loop subdivision centered around an even vertex f_0. The local neighborhood is shown for 1-ring of the trial coarse vertices $\widetilde{c}_i$. Trial residuals are denoted by $\widetilde{r}_i$.

These masks define the mask P of the Loop subdivision in the local neighborhood. Based on the trial Loop MR masks of constrained wavelets [22], detail vectors are simply defined as

$$\widetilde{d}_0 = f_0 - (1 - n\beta)\widetilde{c}_0 + \beta \sum_{i=1}^{n} \widetilde{c}_i \qquad (23)$$

for even vertices and

$$\widetilde{d}_i = f_i - \left(\frac{3}{8}(\widetilde{c}_0 + \widetilde{c}_i) + \frac{1}{8}(\widetilde{c}_{i-1} + \widetilde{c}_{i+1}) \right) \qquad (24)$$

for neighboring odd vertices (i = 1, 2, ..., n).

This means that the initial setting for the details $\widetilde{d}_i$ is the same as the trial residuals $\widetilde{r}_i$. To achieve an economic representation for the details, they are constrained such that details at even vertices can be found from a linear combination of the details at adjacent odd vertices. Using this condition as

17

described in [22], we obtain

$$\widetilde{d}_0 = \frac{8\beta}{5} \sum_{i=1}^{n} \widetilde{d}_i. \tag{25}$$

Therefore, the wavelets coefficients are a subset of $\widetilde{d}_i$ (associated to odd vertices). In addition, Eq. (25) helps to define $\widetilde{A}$ for finding trial coarse vertices as

$$\widetilde{c}_0 = \frac{5}{5 - 8n\beta} f_0 - \frac{8\beta}{5 - 8n\beta} \sum_{i=1}^{n} f_i. \tag{26}$$

These trial coarse vertices neither satisfy minimization (in a local sense) of the subdivision error nor minimization of an estimate of the energy. We would like to refine the position of $\widetilde{c}_0$ to its final position $c_0 = \widetilde{c}_0 + \delta_0$ to minimize a weighted combination of the subdivision error and a local estimate of the surface energy. Similar to the curve case, we keep the position of the neighbors of c_0 fixed. Therefore, the subdivision error around c_0 is defined as sum of the magnitudes of the final residuals (differences between fine vertices f_i and subdivided coarse vertices $\widetilde{f}_i$) in the local neighborhood. Using perturbation vector δ_0 we can represent this error in terms of the trial residuals

$$
\begin{aligned}
E_{subdiv}(\delta_0) &= \|\widetilde{r}_0 - (1 - n\beta)\delta_0\|_2^2 + \\
&\quad \|\widetilde{r}_1 - \frac{3}{8}\delta_0\|_2^2 + \ldots + \|\widetilde{r}_n - \frac{3}{8}\delta_0\|_2^2.
\end{aligned} \tag{27}
$$

Using the direct connection between residuals and detail vectors (Eq. (23) and (24)) and Eq. (25) we can find a compact representation for Eq. (27) as

$$
\begin{aligned}
E_{subdiv}(\delta_0) &= \left(n\frac{9}{64} + (1 - n\beta)^2 \right) \|\delta_0\|_2^2 \\
&\quad - \left(2(1 - n\beta)\widetilde{d}_0 + \frac{3}{4} \sum_{i=1}^{n} \widetilde{d}_i \right) \delta_0 + \sum_{i=0}^{n} \left\|\widetilde{d}_i\right\|_2^2.
\end{aligned} \tag{28}
$$

To include the energy term into the minimization model we need to approximate the surface energy at the final coarse points. We use discrete Laplacian operator [38] as an approximation of the energy at c_0. As shown
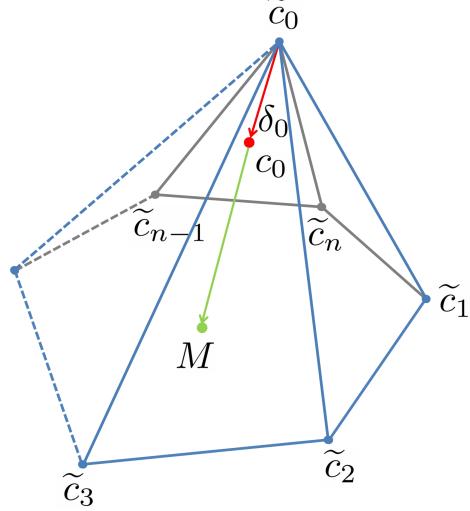
18

Figure 8: Discrete Laplacian vector (green) and the refinement vector (red) for a 1-ring of the trial coarse points.

in Fig. 8, Laplacian operator is defined as a vector from c_0 to the center of the neighboring trial coarse points

$$M = \frac{1}{n} \sum_{i=1}^{n} \widetilde{c}_i. \tag{29}$$

Therefore, by perturbing $\widetilde{c}_0$ to $\widetilde{c}_0 + \delta$ we can minimize the approximation of the energy part as

$$E_{energy}(\delta_0) = \left\| \left(\frac{1}{n} \sum_{i=1}^{n} \widetilde{c}_i \right) - (\widetilde{c}_0 + \delta_0) \right\|_2^2. \tag{30}$$

Now we can use E_{energy} and E_{subdiv} in the weighted least squares formulation of Eq. (6) to find the refinement vector δ_0 as

$$\delta_0 = \frac{\left(\frac{8\beta}{5} \omega(1 - n\beta) + \frac{3}{8}\omega \right) \sum_{i=1}^{n} \widetilde{d}_i}{\omega(n\frac{9}{64} + (1 - n\beta)^2) + (1 - \omega)} +$$

$$\frac{\frac{(1-w)}{n} \sum_{i=1}^{n} \widetilde{c}_i - (1 - \omega)\widetilde{c}_0}{\omega \left(n\frac{9}{64} + (1 - n\beta)^2 \right) + (1 - \omega)}. \tag{31}$$

Algorithm 1 Smooth reverse Loop subdivision

Input: F, ω and local multiresolution masks of P, $\widetilde{Q}$, $\widetilde{A}$ and $\widetilde{B}$

  1: $\widetilde{C} = \widetilde{A}F$ as shown in Eq. (26)

  2: $\widetilde{D} = \widetilde{B}F$ as shown in Eq. (24) and Eq. (25)

  3: δ_0 = Solution of the least squares (6) using Eq. (28) and Eq. (30) as shown in Eq. (31)

  4: $c_0 = \widetilde{c}_0 + \delta_0$

Output: c_0

Algorithm 1 summarizes the decomposition step of smooth reverse Loop subdivision in a local neighborhood. We only need to solve the least squares (6) one time for the local neighborhood. After that, by moving the center of the local neighborhood to all $\widetilde{c}_i$ and using the mask of δ_0, the final C is determined. Since the energy of C is minimized, we can have details that better approximate characteristics of the high-resolution mesh. After finding C, the final residuals can be found from Eq. (7) to be used in synthesizing applications.

To have a compact representation for the reconstruction (Eq. (8)) we can just use the trial decomposition filters of the constrained wavelets. Then after decomposition we can replace the even vertices with their corresponding coarse vertex and odd vertices with details. Even details can be computed from their neighboring odd details using Eq. (25).

Fig. 9(a) shows a mesh with 5,888 faces and its second level of decomposition using reverse Loop subdivision approach introduced by Li et al. [21] (see Fig. 9(b)) and smooth reverse Loop subdivision approach (see Fig. 9(c)). As shown, our approach minimizes the energy of the coarse vertices while preserving the overall structure of the mesh. However, Li et al.'s masks create some unwanted artifacts at sharp edges and magnify the scale of the mesh. This makes it hard to edit the fine mesh using Fig. 9(b).

In the Loop subdivision if the mesh contains boundary vertices, we subdivide them using cubic B-spline scheme. Thus for smooth reverse Loop subdivision, boundary treatment can be achieved using local cubic B-spline smooth reverse subdivision approach discussed in section 3.2.

4.2. Catmull-Clark subdivision

Catmull-Clark subdivision [5] is a C^2-continuous scheme based on the cubic B-spline for arbitrary meshes (no restriction on the valence of vertices
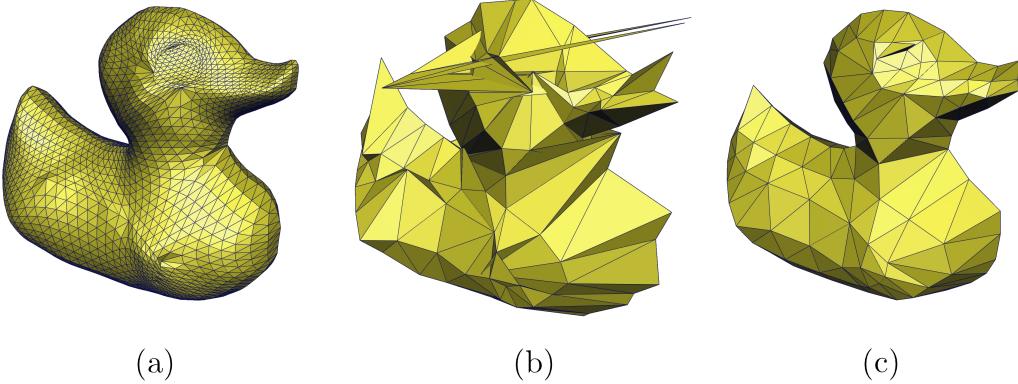
Figure 9: (a) A mesh with $5,888$ faces and its second level of decomposition using (b) Li et al.'s reverse Loop subdivision and (c) smooth reverse Loop subdivision.

or faces). After one level of Catmull-Clark subdivision, all of the faces on the new mesh will consist only of quads.

Based on the general approach discussed in section 3.1 in order to construct local smooth reverse subdivision we should start from a set of trial masks P, $\widetilde{Q}$, $\widetilde{A}$ and $\widetilde{B}$ in a local neighborhood. We start from trial Catmull-Clark masks provided by Olsen and Samavati [23] and refine them toward our optimization goals. Since Catmull-Clark subdivision supports wider range of surfaces, the subdivision masks are more complex than Loop subdivision. As shown in Fig. 10 the 1-ring neighborhood of a *vertex-vertex* v^k at level k with valence n consists of the *edge-vertices* e_i^k and *face vertices* $f_{i,j}^k$. After one level of subdivision, the 1-ring neighborhood of v^{k+1} contains edge vertices e_i^{k+1} and face vertices f_i^{k+1}.

The subdivision masks of Catmull-Clark subdivision are represented as

$$f_i^{k+1} = \frac{1}{n_i^f}\left(v^k + e_i^k + e_{i+1}^k + \sum_j f_{i,j}^k\right) \tag{32}$$

$$e_i^{k+1} = \frac{1}{4}\left(v^k + e_i^k + f_{i-1}^{k+1} + f_i^{k+1}\right) \tag{33}$$

$$v^{k+1} = \frac{n-2}{n}v^k + \frac{1}{n^2}\sum_i e_i^k + \frac{1}{n^2}\sum_i f_i^{k+1} . \tag{34}$$

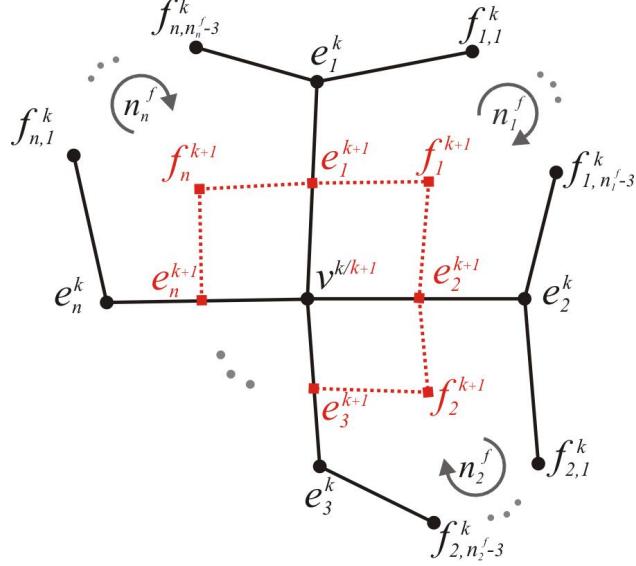In this notation the vertex-vertex mask in Eq. (34) is considered as the

Figure 10: Notation for the neighborhood of v^k and v^{k+1}. The 1-ring neighborhood of v^k consists of e_i^k and $f_{i,j}^k$. The 1-ring neighborhood of v^{k+1} consists of e_i^{k+1} and f_i^{k+1}.

even mask and the edge-vertex mask in Eq. (33) and the face-vertex mask in Eq. (32) are considered as the *odd* masks of the P in the local neighborhood. By rewriting the Eq. (34) as $v^{k+1} = \frac{n-3}{n} v^k + \frac{4}{n^2} \sum_i e_i^{k+1} - \frac{1}{n^2} \sum_i f_i^{k+1}$ the corresponding vertex-, edge- and face- details are expressed as

$$
\widetilde{d}^v \;=\; v^{k+1} - \left(\frac{n-3}{n} \widetilde{v}^k + \frac{4}{n^2} \sum_i \widetilde{e}_i^{k+1} - \frac{1}{n^2} \sum_i \widetilde{f}_i^{k+1} \right) \tag{35}
$$

$$
\widetilde{d}_i^e \;=\; e_i^{k+1} - \widetilde{e}_i^{k+1} \tag{36}
$$

$$
\widetilde{d}_i^f \;=\; f_i^{k+1} - \widetilde{f}_i^{k+1} \tag{37}
$$

where $\widetilde{v}^k$ is the coarse approximation and $\widetilde{e}_i^{k+1}$ and $\widetilde{f}_i^{k+1}$ are resulted from the subdivision of the coarse mesh. Olsen and Samavati [23] utilize the even-odd distinction of the vertices to find the details at even vertices from a linear combination of the details at neighboring odd vertices as

$$
\widetilde{d}^v = \frac{4}{n^2} \sum_i \widetilde{d}_i^e - \frac{1}{n^2} \sum_i \widetilde{d}_i^f \; , i = 1, 2, \ldots, n. \tag{38}
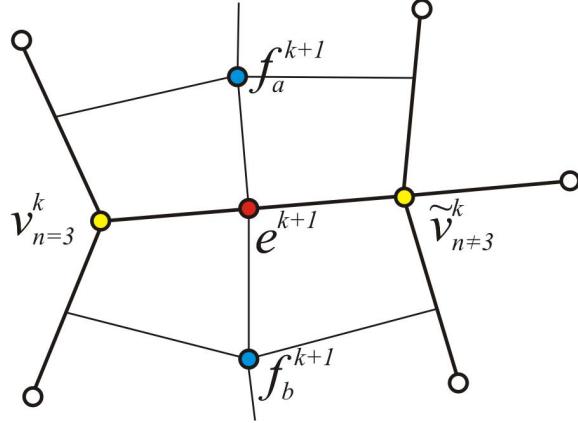$$

Figure 11: Decomposition of a valence-3 vertex $v_{n=3}^k$ using a non-valence-3 neighbor $\widetilde{v}_{n\neq3}^k$ at the coarse level and fine vertices f_a^{k+1}, f_b^{k+1} and e^{k+1}.

Using this constraint, the $\widetilde{A}$ mask for finding trial coarse vertices is given as

$$\widetilde{v}^k = \frac{n}{n-3}v^{k+1} - \frac{4}{n(n-3)}\sum_i e_i^{k+1} + \frac{1}{n(n-3)}\sum_i f_i^{k+1}. \qquad (39)$$

It should be noted that Eq. (39) is not defined when valence of v^k is three ($n = 3$). An alternative solution is to violate the wavelet constraint and explicitly store details for each of these vertices. Fig. 11 shows a valence-3 vertex $v_{n=3}^k$ with one of its non-valence-3 coarse neighbors $\widetilde{v}_{n\neq3}^k$. By reversing the edge subdivision mask of Eq. (33) and using the Eq. (39) for decomposition of $\widetilde{v}_{n\neq3}^k$, an approximation of $v_{n=3}^k$ can be found as

$$v_{n=3}^k \approx 4e^{k+1} - \widetilde{v}_{n\neq3}^k - f_a^{k+1} - f_b^{k+1} . \qquad (40)$$

This approximation can be enhanced by averaging the results of Eq. (40) for all adjacent $v_{n\neq3}^k$ vertices. However, because of storing an explicit detail vector for $v_{n=3}^k$ the detail constraint is violated.

Now that a trial representation for the coarse vertices is found, we can refine them to satisfy minimization of the subdivision error as well as minimization of the discrete local energy. In our refinement step we replace $\widetilde{v}^k$ by $v^k = \widetilde{v}^k + \delta$ to satisfy these two goals. Subdivision error is represented as sum of the differences between fine vertices and subdivision of the refined

23

coarse vertices

$$
\begin{aligned}
E_{subdiv}(\delta) &= \|d^v\|_2^2 + \sum_i \|d_i^e\|_2^2 + \sum_i \|d_i^f\|_2^2 \\
&= \|\widetilde{d^v} - r\delta\|_2^2 + \sum_i \|\widetilde{d_i^e} - s_i\delta\|_2^2 + \sum_i \|\widetilde{d_i^f} - t_i\delta\|_2^2 \quad (41)
\end{aligned}
$$

where

$$
r = \frac{n-2}{n} + \frac{1}{n^2}\sum_i \frac{1}{n_i^f} \tag{42}
$$

$$
s_i = \frac{1}{4}\left(1 + \frac{1}{n_i^f} + \frac{1}{n_{i-1}^f}\right) \tag{43}
$$

$$
t_i = \frac{1}{n_i^f} \tag{44}
$$

and $\widetilde{d^v}$, $\widetilde{d_i^e}$ and $\widetilde{d_i^f}$ are resulted from Eq. (35), (36) and (37).

Eq. (41) can be simplified to

$$
\begin{aligned}
E_{subdiv}(\delta) &= \left(r^2 + \sum_i s_i^2 + \sum_i t_i^2\right)\|\delta\|_2^2 - 2\left(r\widetilde{d^v} + \sum_i s_i\widetilde{d_i^e} + t_i\widetilde{d_i^f}\right)\cdot\delta + \\
&\quad \left(\|\widetilde{d^v}\|_2^2 + \sum_i \|\widetilde{d_i^e}\|_2^2 + \sum_i \|\widetilde{d_i^f}\|_2^2\right) . \tag{45}
\end{aligned}
$$

To minimize the energy of the coarse points around v^k we use discrete Laplacian operator [28] for v^k and its adjacent edge-vertices $\widetilde{e}_i^k$ as

$$
E_{energy}(\delta) = \left\|\left(\frac{1}{n}\sum_i \widetilde{e}_i^k\right) - (\widetilde{v}^k + \delta)\right\|_2^2 . \tag{46}
$$

Now by using E_{subdiv} and E_{energy} in Eq. (6) and utilizing the detail constraint (Eq. (38)) the refinement vector δ can be found as

$$
\delta = \frac{\sum(\frac{4\omega}{n^2}r + \omega s_i)d_i^e + \sum(\frac{-\omega}{n^2}r + \omega t_i)d_i^f + \frac{1-w}{n}\sum \widetilde{e}_i^k - (1-\omega)\widetilde{v}^k}{\omega\left(r^2 + \sum s_i^2 + \sum t_i^2\right) + (1-\omega)} . \tag{47}
$$

In the refinement step we assume that the neighbors of the central vertex $\widetilde{v}^k$ are fixed. Therefore, we can find the final coarse mesh by moving the
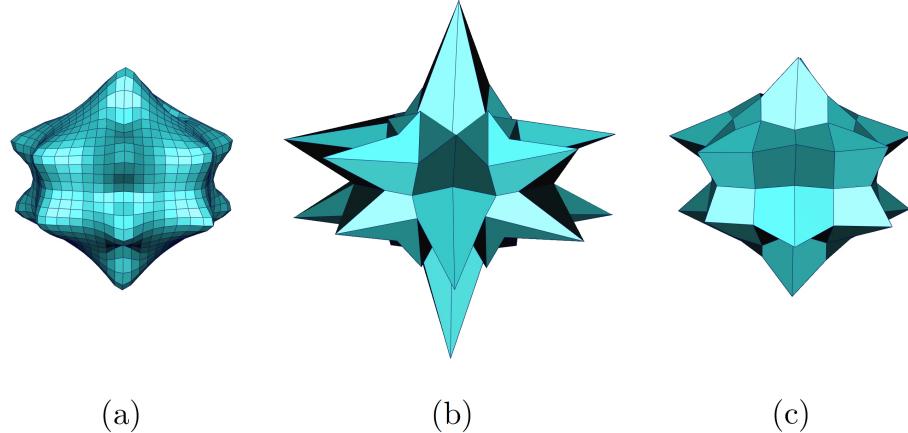
Figure 12: (a) A mesh with $1,536$ faces and its second level of decomposition using (b) Bertram et al.'s Catmull-Clark MR system and (c) smooth reverse Catmull-Clark subdivision.

center of our local neighborhood to all other $\widetilde{v}^k$ except valence-3 vertices. For valence-3 vertices we observed that it is better to ignore E_{subdiv} and only use E_{energy} in Eq. (6). After solving the resulted least squares formulation, the perturbation vector δ for valence-3 vertices is determined as

$$\delta = \left(\frac{1}{n} \sum_i \widetilde{e}_i^k \right) - \widetilde{v}^k. \tag{48}$$

Now that the coarse mesh C is found, we can find the final residuals from Eq. (7). Decomposition step of smooth reverse Catmull-Clark subdivision can be summarized in a similar way to algorithm 1.

Fig. 12(a) shows a mesh with $1,536$ faces and its second level of decomposition using Catmull-Clark MR system described by Bertram et al. [20] (see Fig. 12(b)) and smooth reverse Catmull-Clark subdivision (see Fig. 12(c)). As shown, Bertram et al.'s approach magnifies the scale of the coarse points while our approach preserves the overall mesh structure. This benefit is resulted from minimization of the energy of the coarse vertices during different levels of resolution. Also our approach stores all of the missing characteristics of the fine mesh in the detail vectors while detail vectors in the other approach contain some extra positional information.

Since Catmull-Clark scheme is based on bi-cubic filters, its boundary treatment is similar to the Loop scheme and we only need to subdivide the

25

boundary vertices using cubic B-spline scheme. Consequently, to handle the boundaries in smooth reverse Catmull-Clark subdivision, we use the local cubic B-spline smooth reverse subdivision approach discussed in section 3.2.

The general approach presented in section 3.1 is flexible enough to be extended to other surface subdivision schemes such as Butterfly subdivision [37, 39] and Doo subdivision [10]. Butterfly is an interpolating surface subdivision scheme and has trivial trial filters as presented diagrammatically in [40]. The trial filters of Doo subdivision are introduced by Samavati et al. at [9].

5. Results and discussion

In this section we present more results of our MR approach and discuss its advantages in surface editing and synthesis applications.

Multiresolution representation allows convenient control of surface editing. We have developed an interactive MR surface editor based on smooth reverse Loop and Catmull-Clark subdivision. It allows decomposition and reconstruction of a surface with subdivision connectivity and provides a few editing tools to manipulate coarse vertices. Fig. 13 shows two decomposition levels of a sample model of a helmet with $1,280$ faces using two different techniques. First row is resulted from smooth reverse Loop subdivision while the second row uses reverse Loop subdivision approach introduced by Li et al. [21]. As shown, the Li et al.'s approach magnifies the sharp vertices during decomposition (see the second row of Fig. 13). Therefore, the overall structure of the coarse approximation in this approach does not match with the overall structure of the original fine mesh. This may give the user an incorrect impression of the scale of editing needed on the coarse surface to achieve a particular scale of feature on the fine surface. However, our smooth reverse Loop subdivision approach (see the first row of Fig. 13) preserves the overall structure of the original surface in the coarse mesh which makes it a better candidate for MR surface editing. For this example we have used $\omega = 0.5$ which usually provides acceptable balance between fitness and smoothness of the coarse mesh at the early decomposition steps.

Fig. 14 provides an example of using our MR surface editor to add an eye to the duck model in Fig. 9(a). We use the second decomposition level of the fine mesh using smooth reverse Loop subdivision (see Fig. 9(c)) with $\omega = 0.6$. As highlighted in Fig. 14(a) we only need to translate one vertex of the coarse mesh to make an impression of the eye (see Fig. 14(b)). Fig. 14(c)
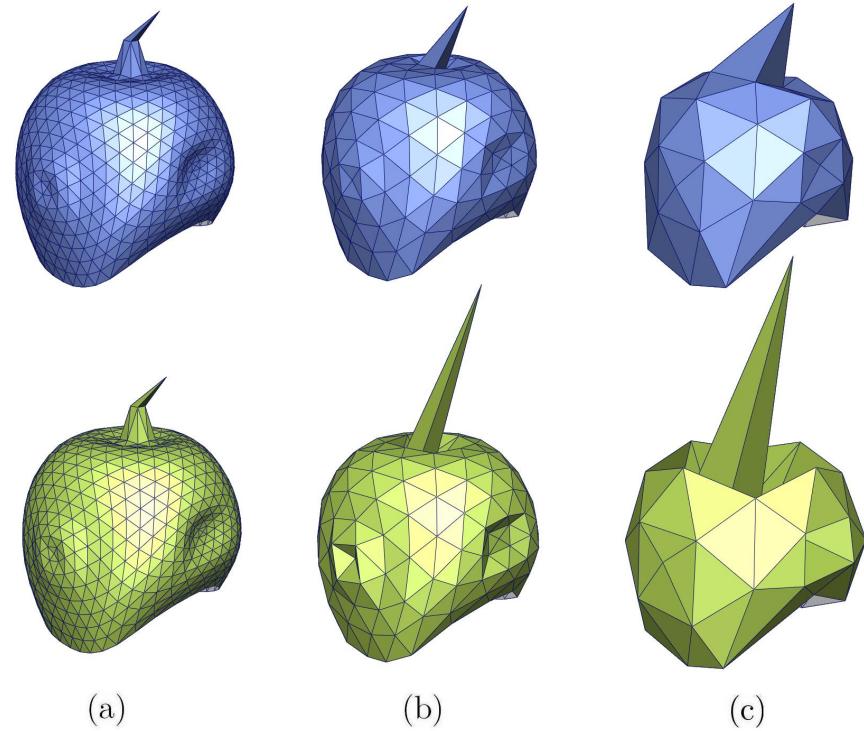
Figure 13: Two levels of decomposition of a mesh using smooth reverse Loop subdivision (first row) and Li et al.'s reverse Loop subdivision (second row).
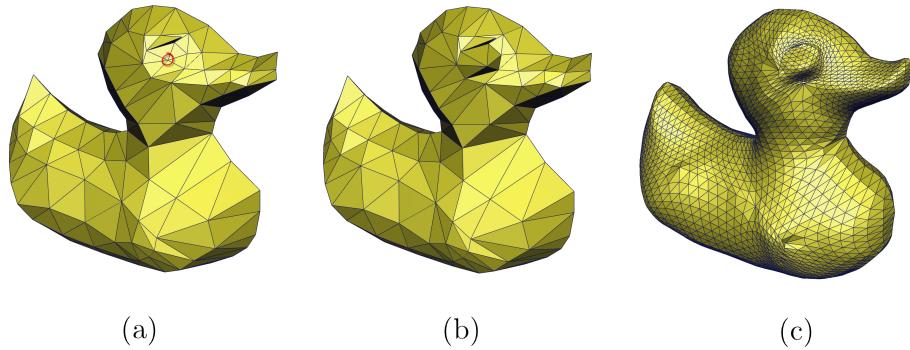

Figure 14: (a) Second decomposition level of the duck model in Fig. 9(a) using smooth reverse Loop subdivision. (b) Editing the highlighted vertex in (a) to add an impression of the eye. (c) The reconstructed model preserves the overall structure of the edited vertex.
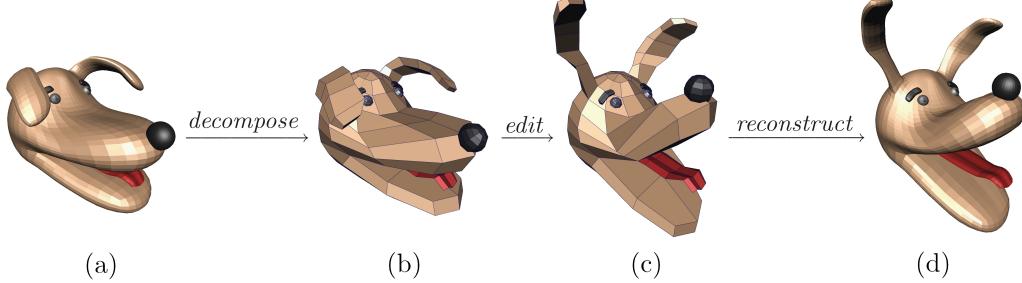
Figure 15: Multiresolution mesh editing: (a) A mesh with $4,960$ faces. (b) Second decomposition level of the mesh using smooth reverse Catmull-Clark subdivision. (c) Editing operations applied to the coarse mesh. (d) The reconstructed model preserves the overall structure of the edited vertices.

shows the result of reconstructing the fine mesh using the edited vertex and detail vectors stored during decomposition. As shown, the new fine vertices preserve the overall structure and scale of the edited coarse vertex. However, it is hard to edit the fine mesh using the coarse vertices resulted from Li et al.'s approach (see Fig. 9(b)). It has some confusing artifacts on the coarse vertices (around the duck's eye) and most importantly it is hard to determine the scale of the perturbations necessary for each coarse point.

Fig. 15 demonstrates another example of using our MR surface editor to edit a mesh with $4,960$ faces. We first decompose the fine mesh in Fig. 15(a) twice using smooth reverse Catmull-Clark subdivision with $\omega = 0.5$. The resulted coarse vertices (see Fig. 15(b)) are then interactively edited to the desired form (see Fig. 15(c)). Fig. 15(d) shows the effect of mesh editing on the reconstructed mesh. As shown, there is a good correspondence between the edited coarse vertices and reconstructed fine vertices which makes our approach suitable for mesh editing applications.

Fig. 16 shows the effect of changing the weighting parameter from 0.0 to 1.0 in decomposition of a mesh with $6,144$ faces. All of the results are from three levels of decomposition using smooth reverse Loop subdivision. This figure demonstrates that decreasing the value of ω generates smoother coarse meshes. On the other hand the overall structure of very smooth coarse meshes has less correspondence with the original mesh. As shown, for this example $\omega = 0.5$ or slightly higher provides a good balance between the smoothness and correspondence. Based on our experiments, the best value of ω lies between 0.5 and 0.75 for smooth reverse Loop Subdivision and between
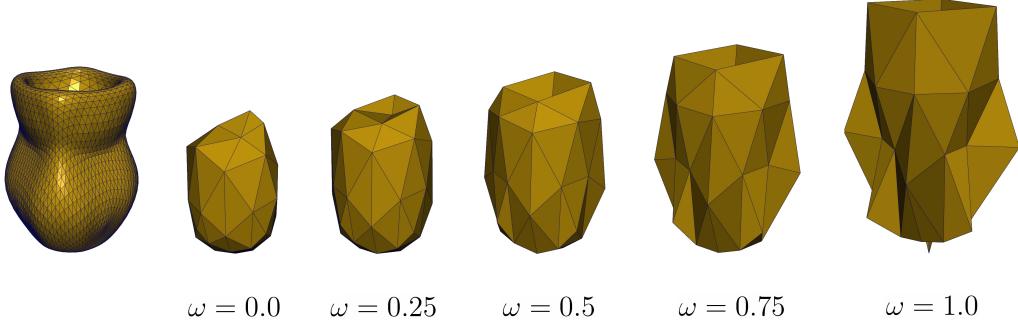
28

Figure 16: Third level of decomposition of a mesh containing $6,144$ faces using smooth reverse Loop subdivision with different weights.

0.25 and 0.5 for smooth reverse Catmull-Clark subdivision. This value can be found in a trial and error approach based on the structure of the fine mesh. When decomposition magnifies the overall structure of the coarse mesh it is better to decrease the value of ω and when it shrinks the coarse mesh the value of ω should be increased. In surface editing applications ω can be adaptively determined for each level of resolution by starting from $\omega = 0.5$ at the first level and incrementing (Loop) or decrementing it (Catmull-Clark) slightly at the next levels. In this way the correspondence between the overall structure of the coarse and fine meshes are better preserved. It should be noted that finding an appropriate weight is a qualitative problem which is highly dependent to the specific application and the complexity of the mesh.

Fig. 17 compares extracting and re-using the detail vectors of a real terrain from USGS [41] with $9,216$ faces (see Fig. 17(a)) using Olsen and Samavati's reverse Catmull-Clark subdivision masks [23] and our smooth reverse Catmull-Clark subdivision approach. In this example, we first decompose the high-resolution mesh in Fig. 17(a) five times and store the detail vectors at different levels of resolution to reach a mesh with 16 vertices. Then we replace the resulted coarse mesh with a 4×4 planar mesh containing 9 faces in order to just visualize the detail vectors. Fig. 17(b) shows the synthesized mesh using Olsen and Samavati's reverse Catmull-Clark subdivision. As shown, a new bump is appeared in the bottom-left side of the mesh which is not the case for the synthesized mesh using our smooth reverse Catmull-Clark subdivision approach (see Fig. 17(c)). This difference is due to the smoothness of the coarser meshes in our approach that helps capturing only the
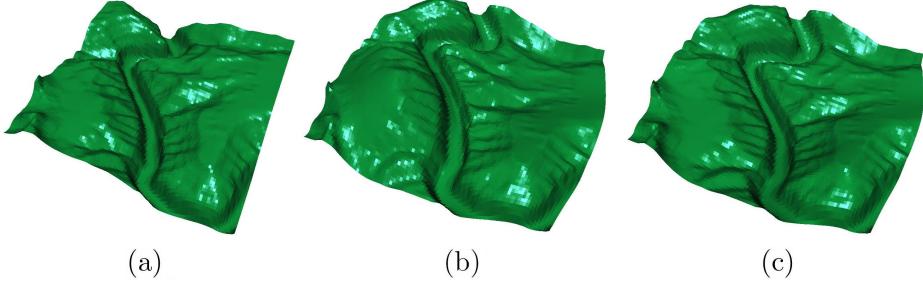
29

Figure 17: (a) A mesh with 9, 216 faces. (b) Detail visualization using reverse Catmull-Clark scheme of Olsen and Samavati. (c) Detail visualization using smooth reverse Catmull-Clark subdivision.

high-frequency characteristics. The coarser meshes in Olsen and Samavati's approach are not smooth; therefore the corresponding details contain extra information. Having details that only contain characteristics information of the surfaces improves the quality of mesh synthesizing and detail transfer applications.

Another benefit of our work is to provide a simple hierarchical structure for residuals in different levels of details. The common surface fairing techniques [14, 30] repeat the Laplacian operator [38] for all of the vertices on the surface and use the Laplacian vectors as details. In Fig. 18 we examine the major deficiency of these approaches by repeating the first order Laplacian operator four times on a sample zigzag curve with 28 points. The left column shows original curve (in red) and its Laplacian result (in blue). Corresponding Laplacian details are shown in the right column (in green). This example indicates that repeating the Laplacian operator does not necessarily create a hierarchical representation (or a multiscale representation) for details. The restriction is that the scale of the details in this technique does not necessarily become smaller after repeating the operator. In addition, general Laplacian representation requires more storage space than our approach. We have the advantage of starting from a trial subdivision scheme with compact representation such as constrained wavelets [22] and achieve separate detail vectors and residual vectors. This is compatible with the general setting of MR while other techniques can only create residual vectors.

Fig. 19 compares the coarsening step of Zorin et al. [15] (the first row) with smooth reverse Loop subdivision (second row). In each row, column (a) shows the initial mesh, column (b) shows the edited mesh and column
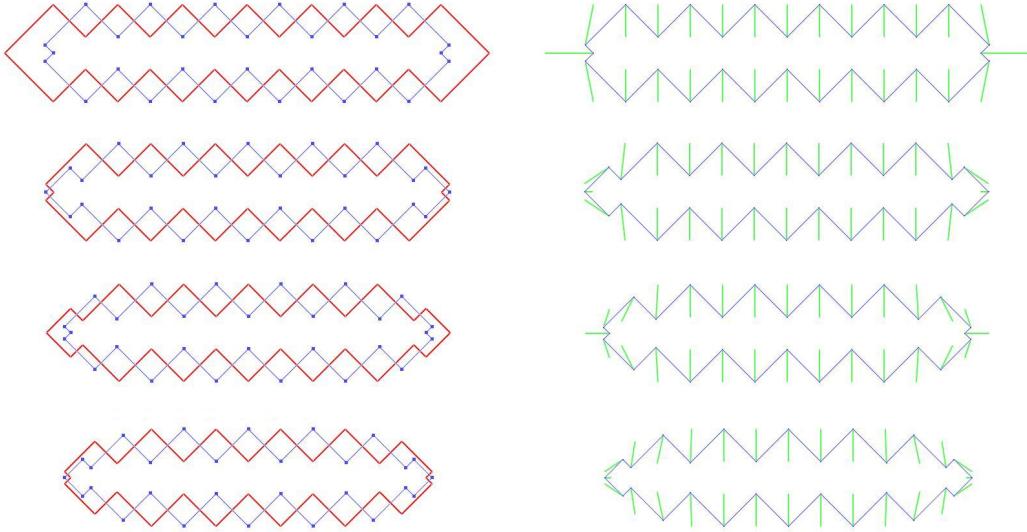
Figure 18: Repeating the first order Laplacian operator on a zigzag curve with 28 points. The left column shows the original curve (in red) and the result of the smoothing (in blue). The right column shows the Laplacian details (in green).

(c) shows the effect of the edit on the coarser level. Since the coarsening step of Zorin et al. is not dual of the subdivision (Loop) it produces some low frequency artifacts. For example a sharp corner can be observed in the lower left corner of their coarse mesh. While in our approach the coarse mesh preserves the same overall structure of the fine mesh. In addition, Zorin et al.'s approach needs significant efforts to achieve good performance because of their complex data structure while all of the underlying operations in our construction are linear in terms of the number of the vertices.

The first two operations in algorithm 1 find trial coarse and trial details in the same order of subdivision operation. Also the least squares formulation in Eq. (6) can be solved once and then be used to calculate all of the perturbation vectors with the same scale of subdivision. In addition, both of the Eq. (7) and Eq. (8) reconstruct the original points linearly. Therefore, all of the necessary operations for decomposition and reconstruction have comparable complexity to the subdivision.

Run-time efficiency is the direct advantage of having linear decomposition and reconstruction operations. Fig. 20 shows a complex model containing $108,608$ faces (see Fig. 20(a)) and its first and second levels of decomposition
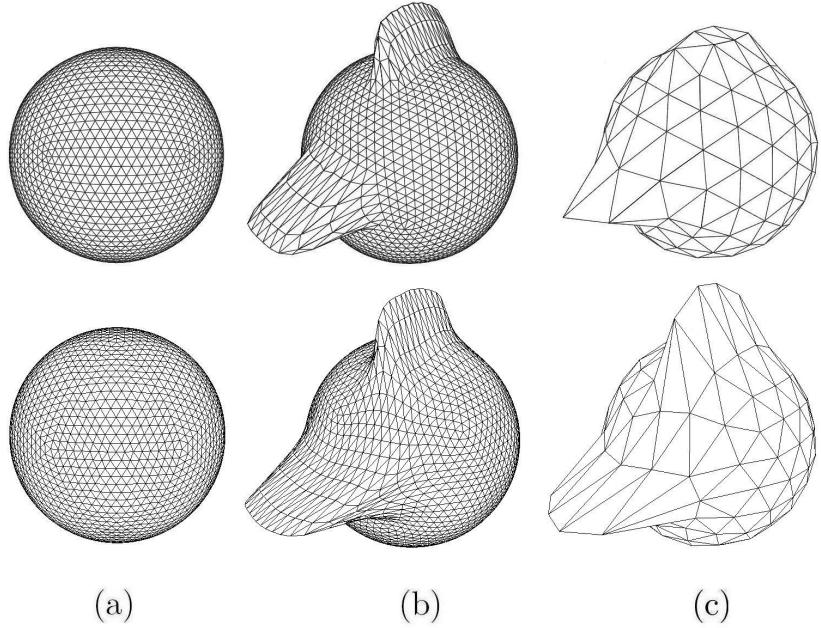
31

Figure 19: Coarsening step of Zorin et al. (first row) and smooth reverse Loop subdivision (second row). (a) The initial mesh. (b) The edited mesh. (c) The coarsening result.
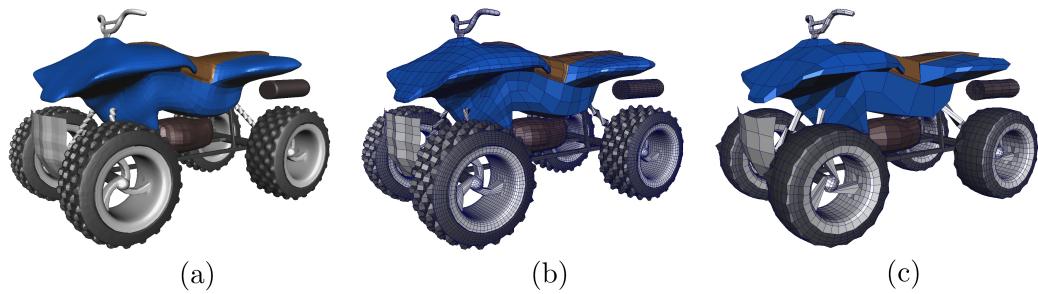

Figure 20: Decomposition of a complex surface: (a) A model with $108,608$ faces. (b) The first and (c) second levels of decomposition using smooth reverse Catmull-Clark subdivision.

Table 1: Summary of the running times (in seconds) of sample decomposition and reconstruction tasks using smooth reverse Loop and Catmull-Clark subdivision.

Model	Decomposition time (s)			Reconstruction time (s)		
	M^1	M^2	M^3	M^2	M^1	M^0
Helmet	0.015	0.007	0.004	0.002	0.005	0.043
Dog	0.146	0.057	-	-	0.046	0.527
Duck	0.084	0.016	-	-	0.051	0.690
Vase	0.093	0.019	0.008	0.005	0.054	0.759
Terrain	0.491	0.074	0.029	0.028	0.365	5.373

using smooth reverse Catmull-Clark subdivision with $\omega = 0.5$. One level of decomposition (see Fig. 20(b)) generates a mesh with $27,152$ faces in 7.26 seconds. Further decomposition (see Fig. 20(c)) results in a mesh with $6,788$ faces in 1.94 seconds. It shows that our approach can reduce the geometric complexity of the original mesh by a factor of 16 in less than 10 seconds, yet the coarse model still preserves the overall structure of the fine model.

Table 1 summarizes decomposition and reconstruction times of a few sample models (from simple to complex). We denote the original mesh as M^0 and the mesh after i levels of decomposition as M^i. All timings are taken on a DELL XPS 420 desktop running Microsoft Windows 7 and equipped with 3.0 GHz CPU and nVIDIA GeForce 8800 GPU. As shown, running time of our approach is real-time for meshes containing a few thousand faces. Since the MR editor is based on a naive half-edge data structure developed in a high-level language (C#), the performance for very complex meshes is less than optimal. Using advanced data structures for subdivision can improve this performance. Despite this overhead, the above mentioned benefits combined with the enhancement of the characteristics of the details make our approach a better solution for interactive MR surface editing and synthesis of complex surfaces.

6. Conclusion

We have presented a new multiresolution technique for general topology surfaces based on reversing the subdivision in a local neighborhood with two goals of finding a good approximation of the fine points and producing

coarse points with minimum energy. Our construction starts from a trial set of multiresolution filters and uses a local least squares formulation to find the refinement vectors that balance between our two optimization goals. The flexibility of our construction allows us to start from any biorthogonal multiresolution setting. We have demonstrated our approach by deriving local smooth reverse subdivision for cubic B-spline scheme. Then we have shown details of extending our approach to general topology surfaces by constructing smooth reverse of the Loop and Catmull-Clark subdivisions.

We have provided different examples to compare the results of our approach with current reverse subdivision techniques. We have also shown benefits of using our approach in a few surface editing and synthesis applications. In future, we plan to extend our approach to support other geometric constraints on curves and surfaces such as visibility. We also plan to use our approach in other feature transfer applications such as motion synthesis by-example. Full exploration of the weight parameter is another interesting future direction.

7. Acknowledgements

References

[1] M. Brunn, M. C. Sousa, F. F. Samavati, Capturing and re-using artistic styles with reverse subdivision-based multiresolution methods, Int. J. Image Graphics 7 (4) (2007) 593–615.

[2] A. Hertzmann, N. Oliver, B. Curless, S. M. Seitz, Curve analogies, in: EGRW '02: Proceedings of the 13th Eurographics workshop on Rendering, 2002, pp. 233–246.

[3] J. Sadeghi, F. F. Samavati, Smooth reverse subdivision, Comput. Graph. 33 (3) (2009) 217–225.

[4] C. Loop, Smooth subdivision surfaces based on triangles, Master's thesis, Department of Mathematics, University of Utah, 1987.

[5] E. Catmull, J. Clark, Recursively generated b-spline surfaces on arbitrary topological meshes, Computer-Aided Design 10 (6) (1978) 350–355.

[6] E. J. Stollnitz, T. D. DeRose, D. H. Salesin, Wavelets for computer graphics: A primer, part 1, IEEE Comput. Graph. Appl. 15 (3) (1995) 76–84.

[7] F. F. Samavati, R. H. Bartels, Multiresolution curve and surface representation: reversing subdivision rules by least-squares data fitting, Computer Graphics Forum 18 (2) (1999) 97–119.

[8] R. H. Bartels, F. F. Samavati, Reversing subdivision rules: local linear conditions and observations on inner products, J. Comput. Appl. Math. 119 (1-2) (2000) 29–67.

[9] F. F. Samavati, N. Mahdavi-Amiri, R. H. Bartels, Multiresolution surfaces having arbitrary topologies by a reverse doo subdivision method, Comput. Graph. Forum 21 (2) (2002) 121–136.

[10] D. Doo, M. Sabin, Behaviour of recursive division surfaces near extraordinary points, Computer-Aided Design 10 (6) (1978) 356 – 360.

[11] A. Finkelstein, D. H. Salesin, Multiresolution curves, in: SIGGRAPH '94: Proceedings of the 21st annual conference on Computer graphics and interactive techniques, 1994, pp. 261–268.

[12] L. Kobbelt, P. Schröder, A multiresolution framework for variational subdivision, ACM Trans. Graph. 17 (4) (1998) 209–237.

[13] J. M. Lounsbery, T. D. DeRose, J. Warren, Multiresolution analysis for surfaces of arbitrary topological type, ACM Transactions on Graphics 16 (1) (1997) 34–73.

[14] L. Kobbelt, S. Campagna, J. Vorsatz, H. peter Seidel, Interactive multiresolution modeling on arbitrary meshes, in: SIGGRAPH '98: Proceedings of the 25th annual conference on Computer graphics and interactive techniques, 1998, pp. 105–114.

[15] D. Zorin, P. Schröder, W. Sweldens, Interactive multiresolution mesh editing, in: SIGGRAPH '97: Proceedings of the 24th annual conference on Computer graphics and interactive techniques, 1997, pp. 259–268.

[16] F. F. Samavati, H. reza Pakdel, C. Smith, Reverse loop subdivision for geometry and textures, Iranian Journal of Mathematical Sciences and Informatics 2 (1) (2007) 21–37.

[17] S. Lanquetin, M. Neveu, Reverse catmull-clark subdivison., in: The 14-th International Conference in Central Europe on Computer Graphics, Visualization and Computer Vision WSCG, Czech Republic, 2006, pp. 25–33.

[18] M. Bertram, Biorthogonal loop-subdivision wavelets, Computing 72 (1-2) (2004) 29–39.

[19] W. Sweldens, The lifting scheme: A construction of second generation wavelets, SIAM Journal on Mathematical Analysis 29 (2) (1998) 511–546.

[20] M. Bertram, M. A. Duchaineau, B. Hamann, K. I. Joy, Bicubic subdivision-surface wavelets for large-scale isosurface representation and visualization, in: IEEE Visualization, 2000, pp. 389–396 & 579.

[21] D. Li, K. Qin, H. Sun, Unlifted loop subdivision wavelets, in: PG '04: Proceedings of the Computer Graphics and Applications, 12th Pacific Conference, 2004, pp. 25–33.

[22] L. Olsen, F. F. Samavati, R. H. Bartels, Multiresolution for curves and surfaces based on constraining wavelets, Computers & Graphics 31 (2007) 449–462.

[23] L. Olsen, F. Samavati, A discrete approach to multiresolution curves and surfaces, in: Transactions on Computational Science VI, Vol. 5730 of Lecture Notes in Computer Science, 2009, pp. 342–361.

[24] D. R. Forsey, R. H. Bartels, Hierarchical b-spline refinement, SIG-GRAPH Comput. Graph. 22 (4) (1988) 205–212.

[25] M. Eck, T. Derose, T. Duchamp, H. Hoppe, M. Lounsbery, W. Stuetzle, Multiresolution analysis of arbitrary meshes, in: In SIGGRAPH 95: Proceedings of the 22nd annual conference on Computer graphics and interactive techniques, 1995, pp. 173–182.

[26] A. W. F. Lee, W. Sweldens, P. Schrder, L. Cowsar, D. Dobkin, MAPS: Multiresolution adaptive parameterization of surfaces, in: Proceedings of SIGGRAPH 98, 1998, pp. 95–104.

[27] H. Biermann, I. Martin, F. Bernardini, D. Zorin, Cut-and-paste editing of multiresolution surfaces, ACM Trans. Graph. 21 (3) (2002) 312–321.

[28] G. Taubin, A signal processing approach to fair surface design, in: Proceedings of 22nd annual conference on computer graphics and interactive techniques, 1995.

[29] O. Sorkine, D. Cohen-Or, Y. Lipman, M. Alexa, C. Rössl, H.-P. Seidel, Laplacian surface editing, in: SGP '04: Proceedings of the 2004 Eurographics/ACM SIGGRAPH symposium on Geometry processing, 2004, pp. 175–184.

[30] L. Kobbelt, J. Vorsatz, H.-P. Seidel, Multiresolution hierarchies on unstructured triangle meshes, Comput. Geom. Theory Appl. 14 (1-3) (1999) 5–24.

[31] L. Olsen, F. F. Samavati, Image-assisted modeling from sketches, in: Proceedings of the Graphics Interface 2010 (GI'10), 2010.

[32] A. Nasri, W. B. Karam, F. Samavati, Sketch-based subdivision models, in: Proceedings of the 6th Eurographics Symposium on Sketch-Based Interfaces and Modeling (SBIM'09), 2009, pp. 53–60.

[33] R. H. Bartels, G. H. Golub, F. F. Samavati, Some observations on local least squares, BIT Numerical Mathematics 46 (3) (2006) 455–477.

[34] F. F. Samavati, R. H. Bartels, L. Olsen, Local b-spline multiresolution with examples in iris synthesis and volumetric rendering, Series in Machine Perception and Artificial Intelligence 67 (3) (2007) 65–102.

[35] A. J. Hanson, H. Ma, Parallel transport approach to curve framing, Tech. rep., Indiana University (1995).

[36] G. M. Chaikin, An algorithm for high-speed curve generation, Computer Graphics and Image Processing 3 (4) (1974) 346 – 349.

[37] N. Dyn, D. Levin, J. A. Gregory, A butterfly subdivision scheme for surface interpolation with tension control, ACM Transactions on Graphics 9 (2) (1990) 160–169.

[38] M. Alexa, Differential coordinates for local mesh morphing and deformation, The Visual Computer 19 (2) (2003) 105 – 114.

[39] D. Zorin, P. Schröder, W. Sweldens, Interpolating subdivision for meshes with arbitrary topology, in: SIGGRAPH '96: Proceedings of the 23rd annual conference on Computer graphics and interactive techniques, 1996, pp. 189–192.

[40] F. F. Samavati, R. H. Bartels, Diagrammatic tools for generating biorthogonal multiresolutions, International Journal of Shape Modeling 12 (1) (2006) 47–73.

[41] U. S. G. S. (USGS), Seamless data distribution system (2010).
URL http://seamless.usgs.gov